High-Yield Growth and Characterization of ⟨100⟩ InP p−n Diode Nanowires

Alessandro Cavalli,[*,†] Jia Wang,[†] Iman Esmaeil Zadeh,[‡] Michael E. Reimer,[‡,§] Marcel A. Verheijen,[†,‖] Martin Soini,[‡] Sebastien R. Plissard,[†,⊥] Val Zwiller,[‡,#] Jos E. M. Haverkort,[†] and Erik P. A. M. Bakkers[†,‡]

[†]Department of Applied Physics, Eindhoven University of Technology, 5600 MB Eindhoven, The Netherlands

[‡]Kavli Institute of Nanoscience, Delft University of Technology, 2628 CJ Delft, The Netherlands

[§]Institute for Quantum Computing and Department of Electrical and Computer Engineering, University of Waterloo, Waterloo, N2L 3G1, Canada

[‖]Philips Innovation Services Eindhoven, 5656 AE Eindhoven, The Netherlands

[⊥]CNRS-Laboratoire d'Analyse et d'Architecture des Systemes (LAAS), Université de Toulouse, 7 avenue du colonel Roche, F-31400 Toulouse, France

[#]Department of Applied Physics, Royal Institute of Technology (KTH), 114 28 Stockholm, Sweden

S *Supporting Information*

ABSTRACT: Semiconductor nanowires are nanoscale structures holding promise in many fields such as optoelectronics, quantum computing, and thermoelectrics. Nanowires are usually grown vertically on (111)-oriented substrates, while (100) is the standard in semiconductor technology. The ability to grow and to control impurity doping of ⟨100⟩ nanowires is crucial for integration. Here, we discuss doping of single-crystalline ⟨100⟩ nanowires, and the structural and optoelectronic properties of p−n junctions based on ⟨100⟩ InP nanowires. We describe a novel approach to achieve low resistance electrical contacts to nanowires via a gradual interface based on p-doped InAsP. As a first demonstration in optoelectronic devices, we realize a single nanowire light emitting diode in a ⟨100⟩-oriented InP nanowire p−n junction. To obtain high vertical yield, which is necessary for future applications, we investigate the effect of the introduction of dopants on the nanowire growth.

KEYWORDS: Nanowire, indium phosphide, 100, diode, p−n junction
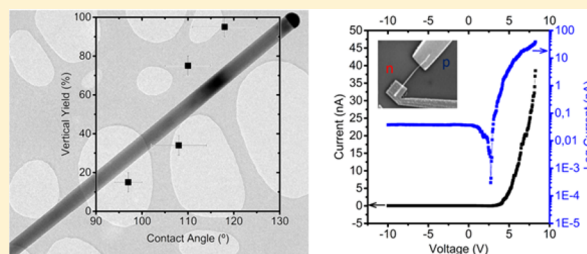
The III−V nanowires (NW) have been shown to provide an ideal platform for the development of nanoscale devices and applications, for example, in quantum computing, energy conversion, and LEDs.[1−6] Nanowires can be grown in a diverse range of crystalline directions on a wide assortment of substrates with different crystal orientations.[7,8] The most common NW growth direction is ⟨111⟩;[9−11] however, in the electronics industry the (100) crystal orientation is the technology standard. The ⟨100⟩ NWs would thus be the best match for present semiconductor fabrication and processing, allowing straightforward integration.[12] A lot of effort has been put in controlling crystal phases in ⟨111⟩ NWs, which remains challenging.[13−15] In contrast, undoped ⟨100⟩ InP NWs always exhibit the pure zincblende (ZB) crystalline structure.[16−20] Up to now; however, devices based on defect-free ⟨100⟩ nanowires have not been demonstrated due to the lack of knowledge about intentional doping of single-crystal ⟨100⟩ NWs. Impurity doping of semiconductors is essential for the functionality of optoelectronic devices.[21,22] In a recent investigation, we showed Au-catalyzed undoped ⟨100⟩ InP NW arrays with high vertical yield, obtained by catalyst engineering.[23] In this report, we study the structural and optoelectronic properties of InP ⟨100⟩

NW-based p−n junctions and investigate the effect of the introduction of dopants during nanowire growth.

We use (100) InP substrates for nanowire growth. Au droplets act as the catalysts for the vapor−liquid−solid (VLS)[24] growth process, while diethyl-zinc (DEZn) and hydrogen sulfide (H₂S) are used as p- and n-dopant precursors during NW growth. Nanowire growth rates in our conditions are approximately 2 nm/s (see Supporting Information S1 for more details). In order to check the possible effect of dopants on the crystalline quality of the NW,[25−27] we studied p−n junctions based on ⟨100⟩ InP nanowires by transmission electron microscopy (TEM, see Supporting Information S2). The growth was performed using a Zn-doped substrate. We introduced the DEZn after 1 min of growth and continued growth for 8 min. Subsequently, we switched off the p-dopant and introduced H₂S, growing for 13 min. The NW shown in Figure 1a has a pure ZB crystal structure without planar defects
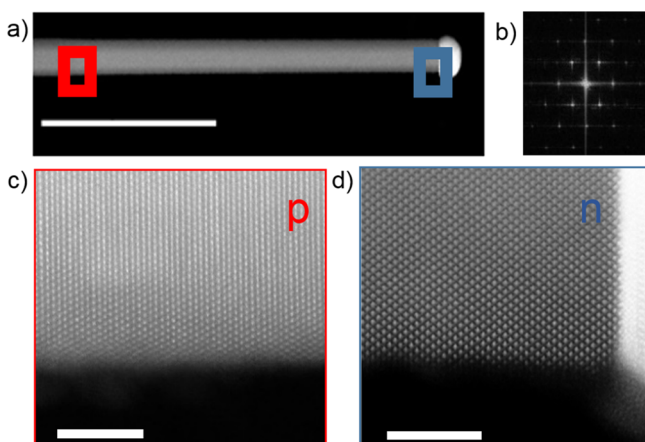
Figure 1. Structural analysis of a ⟨100⟩ p–n junction NW. (a) HAADF STEM image showing an overview image of a p–n-doped ⟨100⟩ InP NW. Dopant molar fractions are 4×10^{-6} (DEZn) and 3×10^{-5} (H$_2$S). Scale-bar is 500 nm. (b) Corresponding FFT image of the NW in panel (a). (c,d) HR-STEM images from the highlighted segments of panel (a), demonstrating the pure zincblende crystalline structure of the NW both for p- and n-doped ⟨100⟩ InP nanowires. Scale bars are 5 nm.

and flat {100} side facets. The corresponding fast Fourier transform (FFT) image in Figure 1b demonstrates the zincblende crystalline structure and confirms the ⟨100⟩ growth direction. To compare, nanowires grown in the ⟨111⟩ direction usually show twin planes, and addition of dopants can completely switch the crystal structure from cubic (for Zn) to hexagonal (for S).[28] In contrast, the ⟨100⟩ InP wires have at most only a few stacking faults per nanowire, always close to the NW base.[23] These defects are stacking faults of {111} planes. A single stacking fault will introduce a kink in the growth direction of the wire. A pair of stacking faults, as observed most frequently, will leave the growth direction unaltered. These defects are introduced during nucleation when the catalyst particle is still evolving toward its equilibrium shape, as has also been discussed in our previous paper.[23] In our case, thus most of the nanowire and, importantly, also the region of the p–n junction is completely free of defects. In ⟨100⟩ nanowires, growth proceeds by nucleation of {100} rather than {111} layers, as in ⟨111⟩ grown nanowires, where the position of the p–n junction is easily recognized by a transition of the crystal phase from zincblende to wurtzite.[28] In the case of ⟨100⟩ nanowires, a change in stacking sequence from cubic (ABC) to hexagonal would imply the introduction of a WZ layer at an angle of 71° with the original growth direction, making this crystal phase transition unlikely. As a result, in ⟨100⟩ NW growth the crystal structure is defect-free ZB for both p- and n-doping (see Figure 1c,d).

After structural characterization, we addressed the electronic properties of doped ⟨100⟩ NWs. The resistance of n-doped NWs, obtained by 4-point probe measurements with Ti/Au metal contacts on a single nanowire, is in the range of a few kiloohms (see Supporting Information S3). This behavior is expected, as Ti/Au contacts have been extensively used for characterization of single n-doped InP NWs.[29] The measured resistance corresponds to a doping concentration of 10^{18} cm^{-3}. In the case of p-doped NWs we used Ti/Zn/Au contacts, which resulted in nonlinear I–V curves if two-point probe measurements are performed. We attribute the observed nonlinear behavior to the formation of Schottky contacts at the metal–

semiconductor nanowire interface, resulting in a potential barrier, which gives rise to the poor electrical contact. The resistance of the nanowires was thus measured by four-point probe measurements to be several tens of megaohms, which corresponds to a doping concentration of $<10^{17}$ cm^{-3} (see Supporting Information S3). Obtaining a low resistive electric contact directly to p-doped InP has previously proven to be a very challenging task.[30,31] In most cases Zn-based metallization is necessary,[32,33] making processing unsuitable for most cleanrooms based on III−V materials or silicon. In particular, the highest active hole concentration accessible by Zn doping of InP has been measured in the $2-5 \times 10^{18}$ cm^{-3} range,[34,35] while the hole concentration necessary to achieve ohmic contacts is predicted to be 5×10^{18} cm^{-3} with conventional Ti/Pt/Au contacts.[36] Furthermore, annealing is often required,[37] adding complexity to the structure and to the processing.

In order to avoid these drawbacks, we developed a contact area that consists of an axial extension of the p-doped InP with p-doped InAs$_x$P$_{1−x}$, where the As content is increased gradually in a continuous linear progression during 15 min of growth until AsH$_3$ and PH$_3$ fractions are the same (Figure 2a). Ohmic contacts can be established on p-doped InAsP and InAs.[38,39] In the top segment of the nanowires, we measured by energy dispersive X-ray spectroscopy (EDS), a fraction of As in the NW increasing from 0 up to 0.56 ± 0.06, which is in good accordance to the molar fractions used. We limited the As content in order to achieve good electrical contacts while maintaining the bandgap large enough as to lower the potential barrier toward the transition to InP where the recombination is intended to occur.

We evaluated the crystalline structure of the NW by TEM measurements (see Supporting Information S2). The growth direction switches from ⟨100⟩ to ⟨111⟩ during the transition from InP to InAsP. The ⟨111⟩ growth direction can be expected to be favored for InAsP NWs unless a careful optimization of growth parameters is accomplished. Here, the InAsP segment is used only as a contact segment and not as an active part of the nanowire devices. Because of the challenges in growing a gradual interface on both the bottom and top of a p-doped NW, we evaluated the performance of the gradual interface only in p–n junctions by measuring I–V characteristics of single nanowires. We grew the NWs in an n-InP/p-InP/p-InAsP growth sequence. To prevent InP noncatalyzed vapor−solid growth, which results in growth of low material quality on the nanowire side facets,[40] we introduced during growth in situ HCl with a molar fraction of 1.8×10^{-5}. However, no HCl was used during the InAsP growth, resulting in a shell that had to be removed after growth (see Supporting Information S1). Measurements on vertical as-grown nanowire devices have been demonstrated previously,[41] but the gradual interface-related kinked morphology makes single vertical nanowire contacting impractical and array processing unfeasible (see Supporting Information). We thus transferred single nanowires to a Si/SiO$_2$ substrate for the electrical measurements and fabricated the metal contacts by two separate steps of electron beam lithography and metal evaporation. We used Ti/Au (110 nm/10 nm) for contacting the n-doped side of the NW and Ti/Pt/Au (1 nm/50 nm/60 nm) for contacting the p-doped side of the NW.

A typical two-point measurement, performed at room temperature, is shown in Figure 2b. We observed similar characteristics at low temperature, where most of the devices have higher voltage thresholds and sharper turn-ons of the
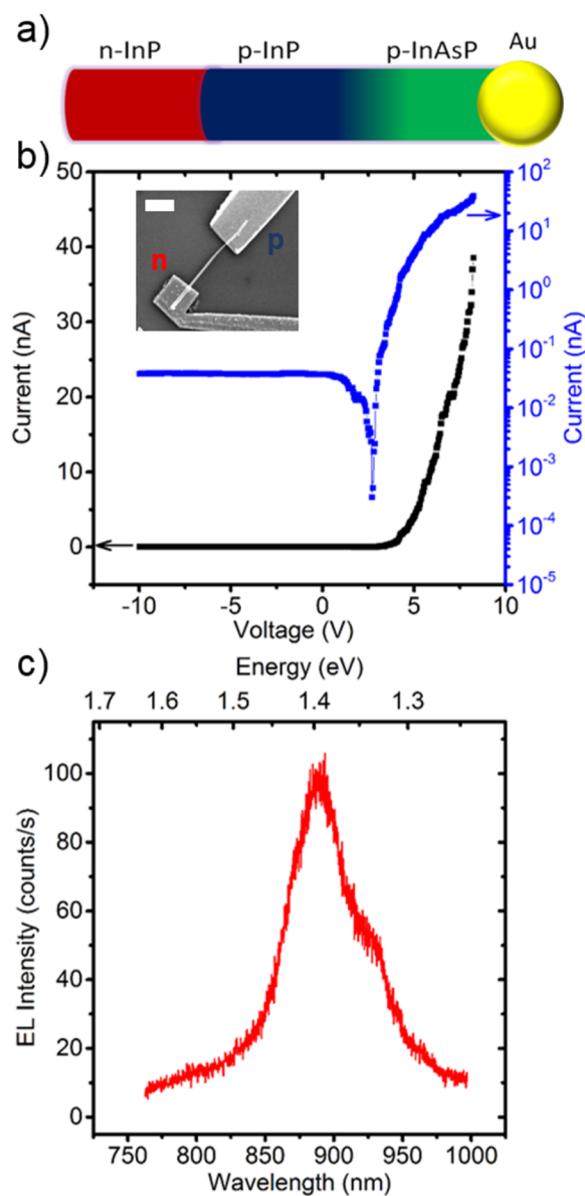
Figure 2. Optoelectronic characterization of p−n junctions based on ⟨100⟩ InP NWs with gradual interface. (a) Scheme of the geometry of single n-InP/p-InP/p-InAsP ⟨100⟩ NW with gradual interface. (b) I−V characterization in dark conditions at room temperature (293 K) of single ⟨100⟩ InP NW p−n junction with the previously described geometry. The current is shown in both a linear and logarithmic scale. Inset: SEM image of device used for NW optoelectronic characterization. Scale bar is 1 μm. (c) EL of single ⟨100⟩ InP NW p−n junction with gradual interface at 4 K, measured at an injection current of 700 nA. Nanowire diameter is 80 nm.

combination of single n-doped and p-doped nanowires, suggesting that ohmic contacts are obtained on both the n- and p-doped regions.

We tested the optoelectronic properties of the nanowire light-emitting diode by electroluminescence, measuring the emission spectrum as a function of the injection current. A typical electroluminescence (EL) spectrum of a single NW, measured at current of 700 nA at a temperature of 4K, is presented in Figure 2c (for more details, see Supporting Information S4). At room temperature, we observed a reduction in EL intensity of the peaks by an order of magnitude. In comparison with p−n junctions based on ⟨111⟩ InP nanowires without gradual interface,[29,42] measured at similar injection currents, the nanowires presented in this work show an order of magnitude stronger peak intensity and narrower peak line-width by a factor of 2. The quantum efficiency at low temperatures is estimated to be ∼0.1%, further indicating an improvement with respect to previously reported devices.[29] At injection levels higher than this, the peak intensity area saturates, resulting in a lower quantum efficiency. Possible channel losses are minority carrier escape to the metal contacts, as the minority carrier diffusion length in InP is >1 μm, and nonradiative recombination due to impurities. We expect the introduction of an undoped segment within the p−n nanowire diode to improve the quantum efficiency for applications of quantum devices. In addition, the nanowire is lying on a substrate with higher refractive index, so a large fraction of the light is directed toward the bottom and is not collected by the objective.[43] Nanowire integration in photonic waveguides can thus also enhance the light extraction efficiency.[44]

Single nanowire devices have limited potential, though as nanowire position control on the wafer scale is essential to develop large-area NW-based devices. A high vertical yield and good reproducibility thus are necessary for future applications. To ensure reproducibility and sample uniformity, Au catalyst particles are patterned via nanoimprint lithography on a 2 inch wafer.[45,46] To study the effect of the addition of dopants on the ⟨100⟩ InP NW growth, we grew p- and n-doped NW on Zn- and S-doped substrates, respectively. In both cases, we switched on the dopant precursor fluxes 10 s after InP growth initiated. At first, we determined the vertical yield, growth rate, and diameter by scanning electron microscopy to gain insight in the morphology of the samples. Using SEM images at 30° tilt, as can be seen in Figure 3a, we measured the growth rate and diameter by averaging at least 15 NWs per sample. For each sample, the vertical yield of five fields of 25 × 25 nanowires from different areas was measured by top-view SEM images (a typical image is shown in the inset of Figure 3a). Nonvertical nanowires are visualized easily in this configuration and include both nanowires growing in the ⟨111⟩ direction and nanowires crawling on the substrate. A very small percentage of gold droplets is absent (<0.01%), resulting in missing NWs in the pattern.

Varying dopant molar fractions over 3 orders of magnitude does not significantly influence the growth rate or the NW diameter, both in the case of Zn- and S-doped wires (see Supporting Information S5). However, the effect of the two dopant types on the vertical yield is completely different. A 3 orders of magnitude variation of the H_2S molar fraction is not changing the vertical yield, which always remains higher than 85%. In contrast, the addition of a small molar fraction of DEZn, subsequently defined as [DEZn], significantly reduces the yield down to 15%. Upon increasing the [DEZn] (from

current. We attribute the relatively high turn-on voltage of 2.5 V to the low Zn doping concentration, which alters significantly the barrier voltage. No saturation of current is observed in the current and voltage range of our measurements (up to 15 V and 2.5 μA, which results in a current density in the order of 10^4 A/cm^2). The rectification ratio (measured in the range of ±5 V) is typically 10^2. We estimated a total series resistance in the device of 1 MΩ, dominated by the series resistance of the p-doped side, which is an improvement of 2 orders of magnitude compared to previous devices.[42] The series resistance is of the same order of magnitude as the resistance measured for the
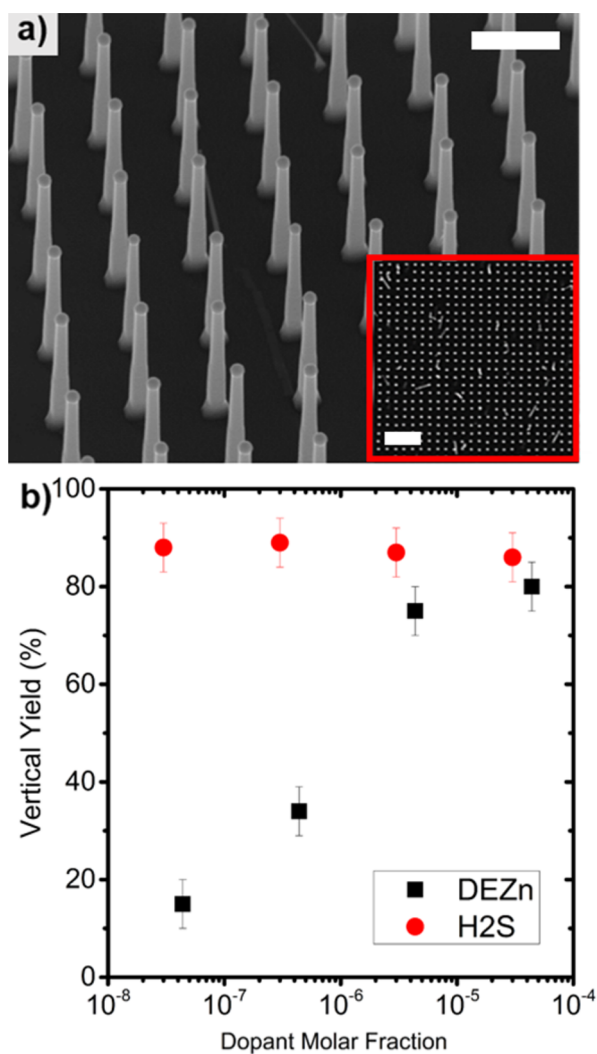
Figure 3. Vertical yield of impurity-doped ⟨100⟩ InP nanowires. (a) A 30° tilt SEM image of p-doped nanowires on p-doped InP substrate patterned by nanoimprint ([DEZn] = 4 × 10⁻⁴, growth conditions described in Supporting Information S1). Scale bar is 500 nm. Inset: Top-view SEM image of nanowires. Scale-bar is 2 μm. (b) Vertical yield of nanowire growth as a function of H_2S (n-dopant) and DEZn (p-dopant) molar fractions.

to the previous growths. After the growth, we cooled down the sample under PH_3 fraction. We studied the contact angle between the gold particle and the nanowire by ex situ side-view SEM, as depicted in the inset of Figure 4b. The contact angle increases from 90 ± 5 to ~125 ± 5° during the first 3 min of growth (Figure 4b). We expect the contact angle to stop increasing after 3 min as contact angles of about 125° have been shown to be ideal for vertical ⟨100⟩ NW growth. Subsequently, the contact angles have been determined for samples grown with different [DEZn] with τ_i = 10 s and terminating the growth after 3 min. We chose τ_i = 10 s as the variation of [DEZn] has the largest effect at this value. The contact angle increases from 97 ± 3 to 117 ± 7° with increasing DEZn molar fraction (Figure 4c). In Figure 4d, we plot the vertical yield versus the contact angle, measured on the same sample: a clear correlation can be observed with the vertical yield increasing with contact angle.

Contact angles in the range of 120−130° have been previously shown to be optimal for vertical growth of undoped ⟨100⟩ NW, because they are close to the dynamic equilibrium of the particle, resulting in stable growth in the ⟨100⟩ direction.[23] The increase of the vertical yield with longer τ_i is thus also explained. A longer τ_i results in a larger contact angle due to the natural evolution of the catalyst particle, which is caused by the line tension, as has been shown previously.[47] Increasing τ_i therefore promotes high vertical yield. Introducing a small amount of DEZn in the early stages of the growth destabilizes the Au droplet, which is very sensitive to any perturbation, causing a reduction in vertical yield. It has already been demonstrated that dopants change the contact angle and the surface energy of catalyst that in this case is Au−In−(Zn,S)[48−50] but these influences have not been unambiguously quantified yet. Our hypothesis originates in the kinetics of VLS growth. We considered a simple model of the catalyst with cylindrical symmetry, similar to what has been proposed previously.[48] Our system is governed by Young's equation at the triple-phase boundary, based on the interplay between surface energies. The addition of Zn is expected to influence all surface energies (γ_{LS}, γ_{LV}, and γ_{SV}, respectively, liquid−solid, liquid−vapor, and solid−vapor). In particular, it is important to point out the influence of Zn on γ_{SV}, which has not been considered extensively before. It has already been demonstrated that DEZn can modify the surface of InP substrates, thus affecting γ_{SV};[51,52] in our case, we expect DEZn to destabilize the catalyst, in particular by increasing its wetting and resulting in a smaller contact angle, by modifying the termination of the (100) InP substrate. There are two contrasting mechanisms expected to act on the catalyst: the first, crucial at high [DEZn], promotes high vertical yield by increasing the catalyst volume and thus the contact angle and affecting the liquid−vapor and liquid−solid interfaces. The second is the effect of DEZn on the surface of InP, which is more significant at low [DEZn] (see Supporting Information S6 for more details). A comprehensive explanation of this phenomenon is beyond the scope of our paper; more detailed studies using, for example, in situ TEM[53] are necessary to conclude definitively on the precise mechanism. A high vertical yield growth of ⟨100⟩ NWs with a wide range of [DEZn] is possible either by growing a relatively short intrinsic stem or by using large [DEZn]. Also, growth of Zn-doped nanowires on S-doped stems behaves in the same way as the growth previously described on undoped segments, making straightforward growing p−n (n−p) junctions.

~10⁻⁷ to 10⁻⁴), the vertical yield increases from 15% to 80% (Figure 3b).

To investigate the effect of DEZn, we have studied p-doped nanowires with a short undoped stem, which have i-p doping profiles. We varied the growth time τ_i of the intrinsic segment before the introduction of the Zn dopant, always keeping a total growth time (τ_i + τ_{doped}) of 8 min. No HCl is used for this study to simplify the growth system, although we did not observe any significant effect on the yield when using HCl. We distinguish two cases: a low (~10⁻⁷) and a high (~10⁻⁴) [DEZn]. For low [DEZn], the vertical yield increases from 15% to about 80% by increasing τ_i from 10 s to 3 min. When a high [DEZn] is used, already a much higher (80%) yield is obtained for τ_i = 10 s, and it increases up to 95% for τ_i = 3 min (Figure 4a).

In order to find the origin of this difference, we have grown a similar series of undoped nanowires without adding the Zn-doped segment, so that the evolution of the catalyst can be studied. Growth times were between 10 s and 3 min, in analogy
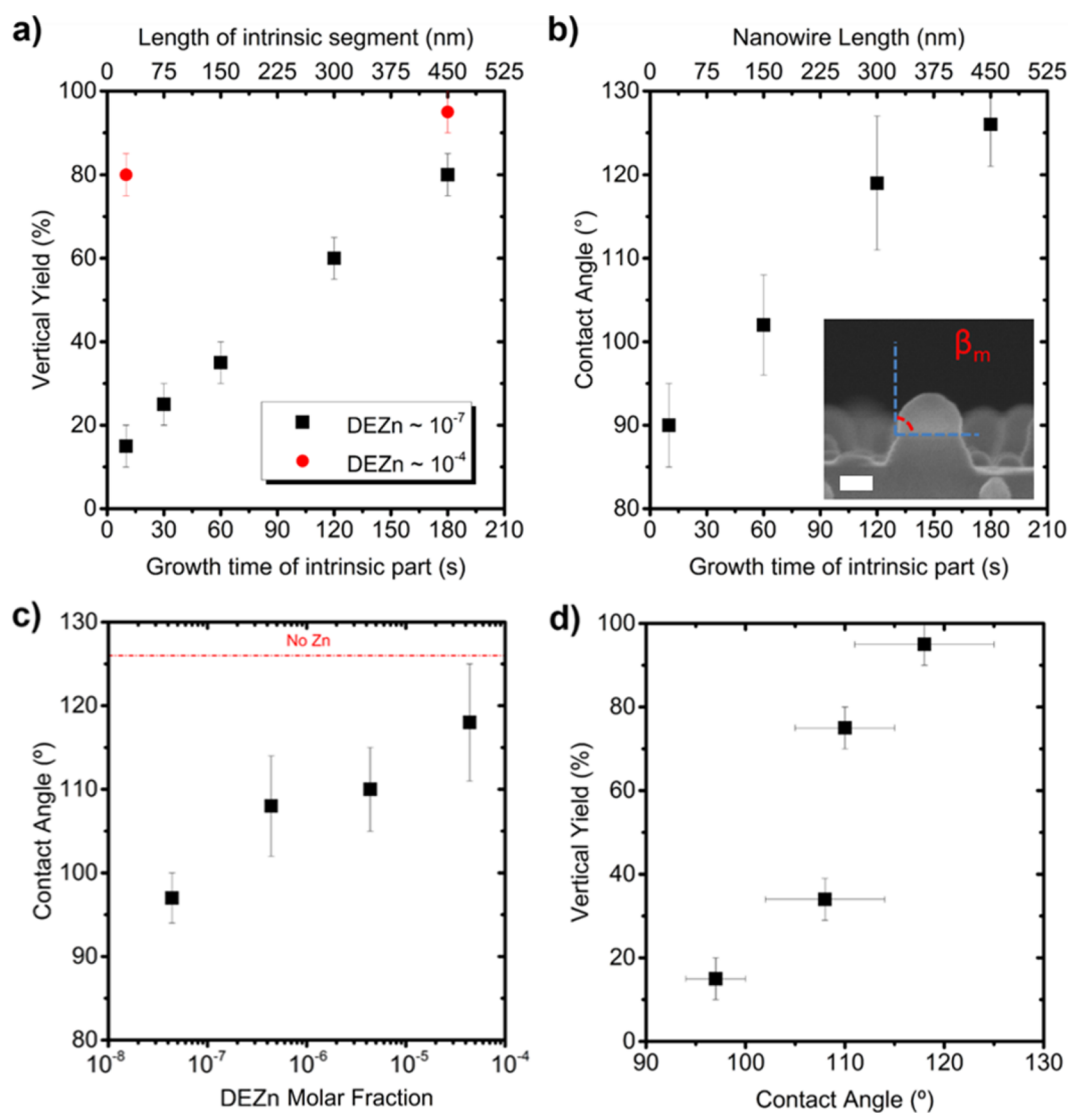
Figure 4. Effect of DEZn on the growth of ⟨100⟩ InP NW. (a) Structure: i-p NW with variable τ_i. Vertical yield of NW with undoped/p-doped segments as a function of τ_i (the growth time of the undoped stem) varied from 10 s to 3 min. (b) Structure: i-NW with variable length. Contact angle of i-InP NW without p-doped segment as a function of τ_i in the same range as panel (a). Inset shows side-view SEM image used to measure ex situ the contact angle between gold particle and NW. Scale bar is 50 nm. (c) Structure: i-p NW with τ_i = 10 s and variable DEZn molar fraction. Contact angle as a function of [DEZn] with τ_i = 10 s. Red dash dot line indicates contact angle if no Zn is introduced. (d) Nanowire vertical yield as a function of contact angle, measured on the same sample as panel (c).

In conclusion, we have demonstrated the first p−n junction based on single-crystalline ⟨100⟩-oriented nanowires and measured its optoelectronic properties in a single-nanowire device. A low resistive contact to p-doped InP has been realized by developing a novel p-InP/p-InAsP gradual interface. To achieve optimal reproducibility and sample uniformity, we have investigated how to obtain high vertical yield of Au-catalyzed p- and n-doped InP NWs grown in the ⟨100⟩ direction. We found that different DEZn molar fractions affect the contact angle between the catalyst droplet and the nanowire. A large contact angle results in a high vertical yield. The ⟨100⟩ nanowires show great potential for next-generation optoelectronics and energy conversion applications, which are integrated with the current semiconductor technology.

■ ASSOCIATED CONTENT

Ⓢ Supporting Information

The Supporting Information is available free of charge on the ACS Publications website at DOI: 10.1021/acs.nano-lett.6b00203.

> Nanowire growth conditions; optoelectronic characterization processing and measurements; SEM and TEM characterization details; gradual interface structural characterization; and doped nanowires growth rate and Zn influence additional discussion. (PDF)

■ AUTHOR INFORMATION

Author Contributions

A.C. and J.W. contributed equally to this work.

Notes

The authors declare no competing financial interest.

■ REFERENCES

(1) Duan, X.; Huang, Y.; Cui, Y.; Wang, J.; Lieber, C. M. Indium Phosphide Nanowires as Building Blocks for Nanoscale Electronic and Optoelectronic Devices. *Nature* **2001**, *409*, 66−69.

(2) Mourik, V.; Zuo, K.; Frolov, S. M.; Plissard, S. R.; Bakkers, E. P. A. M.; Kouwenhoven, L. P. Signatures of Majorana Fermions in Hybrid Superconductor-Semiconductor Nanowire Devices. *Science* **2012**, *336* (80), 1003−1007.

(3) Hochbaum, A. I.; Yang, P. Semiconductor Nanowires for Energy Conversion. *Chem. Rev.* **2010**, *110*, 527−546.

(4) Doh, Y.-J.; van Dam, J. A.; Roest, A. L.; Bakkers, E. P. A. M.; Kouwenhoven, L. P.; De Franceschi, S. Tunable Supercurrent through Semiconductor Nanowires. *Science* **2005**, *309*, 272−275.

(5) Tian, B.; Zheng, X.; Kempa, T. J.; Fang, Y.; Yu, N.; Yu, G.; Huang, J.; Lieber, C. M. Coaxial Silicon Nanowires as Solar Cells and Nanoelectronic Power Sources. *Nature* **2007**, *449*, 885−889.

(6) Duan, X.; Huang, Y.; Agarwal, R.; Lieber, C. M. Single-Nanowire Electrically Driven Lasers. *Nature* **2003**, *421*, 241−245.

(7) Fortuna, S. A.; Li, X. Metal-Catalyzed Semiconductor Nanowires: A Review on the Control of Growth Directions. *Semicond. Sci. Technol.* **2010**, *25*, 024005.

(8) Stekolnikov, A.; Furthmüller, J.; Bechstedt, F. Absolute Surface Energies of Group-IV Semiconductors: Dependence on Orientation and Reconstruction. *Phys. Rev. B: Condens. Matter Mater. Phys.* **2002**, *65*, 115318.

(9) Seifert, W.; Borgström, M.; Deppert, K.; Dick, K. A.; Johansson, J.; Larsson, M. W.; Mårtensson, T.; Skold, N.; Svensson, C. P. T.; Wacaser, B. A.; et al. Growth of One-Dimensional Nanostructures in MOVPE. *J. Cryst. Growth* **2004**, *272*, 211−220.

(10) Assali, S.; Zardo, I.; Plissard, S.; Kriegner, D.; Verheijen, M. A.; Bauer, G.; Meijerink, A.; Belabbes, A.; Bechstedt, F.; Haverkort, J. E. M.; et al. Direct Band Gap Wurtzite Gallium Phosphide Nanowires. *Nano Lett.* **2013**, *13*, 1559−1563.

(11) Tomioka, K.; Yoshimura, M.; Fukui, T. A III−V Nanowire Channel on Silicon for High-Performance Vertical Transistors. *Nature* **2012**, *488*, 189−192.

(12) Borg, M.; Schmid, H.; Moselund, K. E.; Signorello, G.; Gignac, L.; Bruley, J.; Breslin, C.; Das Kanungo, P.; Werner, P.; Riel, H. Vertical III-V Nanowire Device Integration on Si(100). *Nano Lett.* **2014**, *14*, 1914−1920.

(13) Dalacu, D.; Mnaymneh, K.; Lapointe, J.; Wu, X.; Poole, P. J.; Bulgarini, G.; Zwiller, V.; Reimer, M. E. Ultraclean Emission from InAsP Quantum Dots in Defect-Free Wurtzite InP Nanowires. *Nano Lett.* **2012**, *12*, 5919−5923.

(14) Gao, Q.; Saxena, D.; Wang, F.; Fu, L.; Mokkapati, S.; Guo, Y.; Li, L.; Wong-Leung, J.; Caroff, P.; Tan, H. H.; et al. Selective-Area Epitaxy of Pure Wurtzite InP Nanowires: High Quantum Efficiency and Room-Temperature Lasing. *Nano Lett.* **2014**, *14*, 5206−5211.

(15) Lehmann, S.; Wallentin, J.; Jacobsson, D.; Deppert, K.; Dick, K. A. A General Approach for Sharp Crystal Phase Switching in InAs, GaAs, InP, and GaP Nanowires Using Only Group V Flow. *Nano Lett.* **2013**, *13*, 4099−4105.

(16) Björk, M. T.; Ohlsson, B. J.; Sass, T.; Persson, A. I.; Thelander, C.; Magnusson, M. H.; Deppert, K.; Wallenberg, L. R.; Samuelson, L. One-Dimensional Heterostructures in Semiconductor Nanowhiskers. *Appl. Phys. Lett.* **2002**, *80*, 1058−1060.

(17) Krishnamachari, U.; Borgstrom, M.; Ohlsson, B. J.; Panev, N.; Samuelson, L.; Seifert, W.; Larsson, M. W.; Wallenberg, L. R. Defect-Free InP Nanowires Grown in [001] Direction on InP (001). *Appl. Phys. Lett.* **2004**, *85*, 2077−2079.

(18) Li, Z. A.; Mller, C.; Migunov, V.; Spasova, M.; Farle, M.; Lysov, A.; Gutsche, C.; Regolin, I.; Prost, W.; Tegude, F. J.; et al. Planar-Defect Characteristics and Cross-Sections of ⟨001⟩, ⟨111⟩, and ⟨112⟩ InAs Nanowires. *J. Appl. Phys.* **2011**, *109*, 114320.

(19) Wang, J.; Plissard, S.; Hocevar, M.; Vu, T. T. T.; Zehender, T.; Immink, G. G. W.; Verheijen, M. A.; Haverkort, J.; Bakkers, E. P. A. M. Position-Controlled [100] InP Nanowire Arrays. *Appl. Phys. Lett.* **2012**, *100*, 053107.

(20) Fonseka, H. A.; Caroff, P.; Wong-Leung, J.; Ameruddin, A. S.; Tan, H. H.; Jagadish, C. Nanowires Grown on InP (100): Growth Directions, Facets, Crystal Structures, and Relative Yield Control. *ACS Nano* **2014**, *8*, 6945−6954.

(21) Borgström, M. T.; Wallentin, J.; Heurlin, M.; Fält, S.; Wickert, P.; Leene, J.; Magnusson, M. H.; Deppert, K.; Samuelson, L. Nanowires with Promise for Photovoltaics. *IEEE J. Sel. Top. Quantum Electron.* **2011**, *17*, 1050−1061.

(22) Wallentin, J.; Borgström, M. T. Doping of Semiconductor Nanowires. *J. Mater. Res.* **2011**, *26*, 2142−2156.

(23) Wang, J.; Plissard, S. R.; Verheijen, M. A.; Feiner, L. F.; Cavalli, A.; Bakkers, E. P. A. M. Reversible Switching of InP Nanowire Growth Direction by Catalyst Engineering. *Nano Lett.* **2013**, *13*, 3802−3806.

(24) Wagner, R. S.; Ellis, W. C. Vapor-Liquid-Solid Mechanism of Single Crystal Growth. *Appl. Phys. Lett.* **1964**, *4*, 89−90.

(25) Algra, R. E.; Verheijen, M. A.; Borgström, M. T.; Feiner, L.-F.; Immink, G.; van Enckevort, W. J. P.; Vlieg, E.; Bakkers, E. P. A. M. Twinning Superlattices in Indium Phosphide Nanowires. *Nature* **2008**, *456*, 369−372.

(26) Borgström, M. T.; Norberg, E.; Wickert, P.; Nilsson, H. A.; Trägårdh, J.; Dick, K. A.; Statkute, G.; Ramvall, P.; Deppert, K.; Samuelson, L. Precursor Evaluation for in Situ InP Nanowire Doping. *Nanotechnology* **2008**, *19*, 445602.

(27) Wallentin, J.; Mergenthaler, K.; Ek, M.; Wallenberg, L. R.; Samuelson, L.; Deppert, K.; Pistol, M. E.; Borgstroöm, M. T. Probing the Wurtzite Conduction Band Structure Using State Filling in Highly Doped InP Nanowires. *Nano Lett.* **2011**, *11*, 2286−2290.

(28) Cui, Y.; Wang, J.; Plissard, S. R.; Cavalli, A.; Vu, T. T. T.; Van Veldhoven, R. P. J.; Gao, L.; Trainor, M.; Verheijen, M. A.; Haverkort, J. E. M.; et al. Efficiency Enhancement of InP Nanowire Solar Cells by Surface Cleaning. *Nano Lett.* **2013**, *13*, 4113−4117.

(29) Minot, E. D.; Kelkensberg, F.; Van Kouwen, M.; Van Dam, J. A.; Kouwenhoven, L. P.; Zwiller, V.; Borgström, M. T.; Wunnicke, O.; Verheijen, M. A.; Bakkers, E. P. A. M. Single Quantum Dot Nanowire LEDs. *Nano Lett.* **2007**, *7*, 367−371.

(30) Perkins, J. H.; O'Keefe, M. F. O.; Miles, R. E.; Snowden, C. M. *Pt and Zn Based Ohmic Contacts to P-Type InP*. In Proceedings of 1994 IEEE 6th International Conference on Indium Phosphide and Related Materials (IPRM); IEEE: Piscataway, NJ, 1994; pp 190−193.

(31) Hwang, S.; Shim, J.; Eo, Y. *Ohmic Contacts of Pd/Zn/Pt(or Pd)/Au Materials to P-Type InP*. In Conference Proceedings - International Conference on Indium Phosphide and Related Materials; IEEE: Piscataway, NJ, 2005; Vol. *2005*, pp 260−262.

(32) Tabatabaie-Alavi, K.; Choudhury, A. N. M. M.; Slater, N. J.; Fonstad, C. G. Gold-Zinc-Gold Plating on Indium Phosphide, Microelectronics. U.S. Patent US4414076 A, 1983.

(33) Nakahara, S.; Gallagher, P. K.; Felder, E. C.; Lawry, R. B. Interaction between Zinc Metallization and Indium Phosphide. *Solid-State Electron.* **1984**, *27*, 557−564.

(34) Vanhollebeke, K.; D'Hondt, M.; Moerman, I.; Van Daele, P.; Demeester, P. Zn Doping of InP, InAsP/InP, and InAsP/InGaAs Heterostructures through Metalorganic Vapor Phase Diffusion (MOVPD). *J. Electron. Mater.* **2001**, *30*, 951−959.

(35) Moon, Y.; Si, S.; Yoon, E.; Kim, S. J. Low Temperature Photoluminescence Characteristics of Zn-Doped InP Grown by Metalorganic Chemical Vapor Deposition. *J. Appl. Phys.* **1998**, *83*, 2261.

(36) Schubert, E. F.; Pinzone, C. J.; Geva, M. Phenomenology of Zn Diffusion and Incorporation in InP Grown by Organometallic Vapor-Phase Epitaxy (OMVPE). *Appl. Phys. Lett.* **1995**, *67*, 700.

(37) Zhang, K.; Tang, H.; Wu, X.; Xu, J.; Li, X.; Gong, H. Improved Au/Zn/Au Ohmic Contacts for P-Type InP. In *Proceedings of SPIE*; Zhou, L., Ed.; International Society for Optics and Photonics: Bellingham, WA, 2007; Vol. *6621*, pp 662118−−662118-7.

(38) Wang, S. H.; Lysczek, E. M.; Liu, B.; Robinson, J. A.; Mohney, S. E. Shallow and Thermally Stable Ohmic Contacts to P-InAsP. *J. Electrochem. Soc.* **2006**, *153*, G479.

(39) Lysczek, E. M.; Mohney, S. E.; Wittberg, T. N. Shallow Ohmic Contacts to P-Type InAs. *Electron. Lett.* **2003**, *39*, 1866.

(40) Borgström, M. T.; Wallentin, J.; Trägårdh, J.; Ramvall, P.; Ek, M.; Wallenberg, L. R.; Samuelson, L.; Deppert, K. In Situ Etching for Total Control over Axial and Radial Nanowire Growth. *Nano Res.* **2010**, *3*, 264−270.

(41) van Weert, M. H. M.; den Heijer, M.; van Kouwen, M. P.; Algra, R. E.; Bakkers, E. P. A. M.; Kouwenhoven, L. P.; Zwiller, V. Surround-Gated Vertical Nanowire Quantum Dots. *Appl. Phys. Lett.* **2010**, *96*, 233112.

(42) Reimer, M. E.; van Kouwen, M. P.; Barkelid, M.; Hocevar, M.; van Weert, M. H. M.; Algra, R. E.; Bakkers, E. P. A. M.; Bjork, M. T.; Schmid, H.; Riel, H.; et al. Single Photon Emission and Detection at the Nanoscale Utilizing Semiconductor Nanowires. *Proc. SPIE* **2010**, *5*, 11.

(43) Bulgarini, G.; Reimer, M. E.; Zwiller, V. Optical Polarization Properties of a Nanowire Quantum Dot Probed along Perpendicular Orientations. *Appl. Phys. Lett.* **2012**, *101*, 111112.

(44) Zadeh, I. E.; Elshaari, A. W.; Jöns, K. D.; Fognini, A.; Dalacu, D.; Poole, P. J.; Reimer, M. E.; Zwiller, V. Deterministic Integration of Single Photon Sources in Silicon Based Photonic Circuits. *Nano Lett.* **2016**, 10.1021/acs.nanolett.5b04709.

(45) Mårtensson, T.; Carlberg, P.; Borgström, M.; Montelius, L.; Seifert, W.; Samuelson, L. Nanowire Arrays Defined by Nanoimprint Lithography. *Nano Lett.* **2004**, *4*, 699−702.

(46) Pierret, A.; Hocevar, M.; Diedenhofen, S. L.; Algra, R. E.; Vlieg, E.; Timmering, E. C.; Verschuuren, M. A.; Immink, G. W. G.; Verheijen, M. A.; Bakkers, E. P. A. M. Generic Nano-Imprint Process for Fabrication of Nanowire Arrays. *Nanotechnology* **2010**, *21*, 065305.

(47) Schmidt, V.; Senz, S.; Gösele, U. The Shape of Epitaxially Grown Silicon Nanowires and the Influence of Line Tension. *Appl. Phys. A: Mater. Sci. Process.* **2005**, *80*, 445−450.

(48) Wallentin, J.; Ek, M.; Wallenberg, L. R.; Samuelson, L.; Deppert, K.; Borgström, M. T. Changes in Contact Angle of Seed Particle Correlated with Increased Zincblende Formation in Doped InP Nanowires. *Nano Lett.* **2010**, *10*, 4807−4812.

(49) Naidich, Y. V.; Krasovskii, V. P.; Chuvashov, Y. N. Influence of Sulfur and Selenium on the Wettability of Zinc Selenide and Sulfide by Molten Metals. *Sov. Powder Metall. Met. Ceram.* **1986**, *25*, 922−924.

(50) Egry, I.; Lohoefer, G.; Jacobs, G. Surface Tension of Liquid Metals: Results from Measurements on Ground and in Space. *Phys. Rev. Lett.* **1995**, *75*, 4043−4046.

(51) Ikejiri, K.; Ishizaka, F.; Tomioka, K.; Fukui, T. Bidirectional Growth of Indium Phosphide Nanowires. *Nano Lett.* **2012**, *12*, 4770−4774.

(52) Kato, M.; Akiyama, T.; Nakamura, K.; Ito, T. Effects of Zn Doping on the Surface Structure and Initial Growth Processes of InP Thin Film Layers on InP(111)B Substrate. *e-J. Surf. Sci. Nanotechnol.* **2015**, *13*, 147−150.

(53) Chou, Y. C.; Hillerich, K.; Tersoff, J.; Reuter, M. C.; Dick, K. A.; Ross, F. M. Atomic-Scale Variability and Control of III-V Nanowire Growth Kinetics. *Science* **2014**, *343* (80), 281−284.